Electronic Supplementary Information

Layered macrocycles with flexibility and tunable dynamic properties for wide-range thermoresponsive color changes

Nano Shioda,[1] Jung-Moo Heo,[2] Bubsung Kim,[2] Hiroaki Imai,[1] Jong-Man Kim,[2,*] Yuya Oaki[1,*]

[1]Department of Applied Chemistry, Faculty of Science and Technology, Keio University, 3-14-1 Hiyoshi, Kohoku-ku, Yokohama 223-8522, Japan.

[2]School of Chemical Engineering, Hanyang University, Seoul 04763, Korea

E-mail: jmk@hanyang.ac.kr, oakiyuya@applc.keio.ac.jp

Contents

Experimental methods

Syntheses of MCDA. The macrocyclic compound **MCDA** was synthesized according to the literature procedures (Scheme S1).[S1, S2] The detailed synthetic protocols for the intermediate ester **7** and **MCDA** are reported in references S1 and S2, respectively.

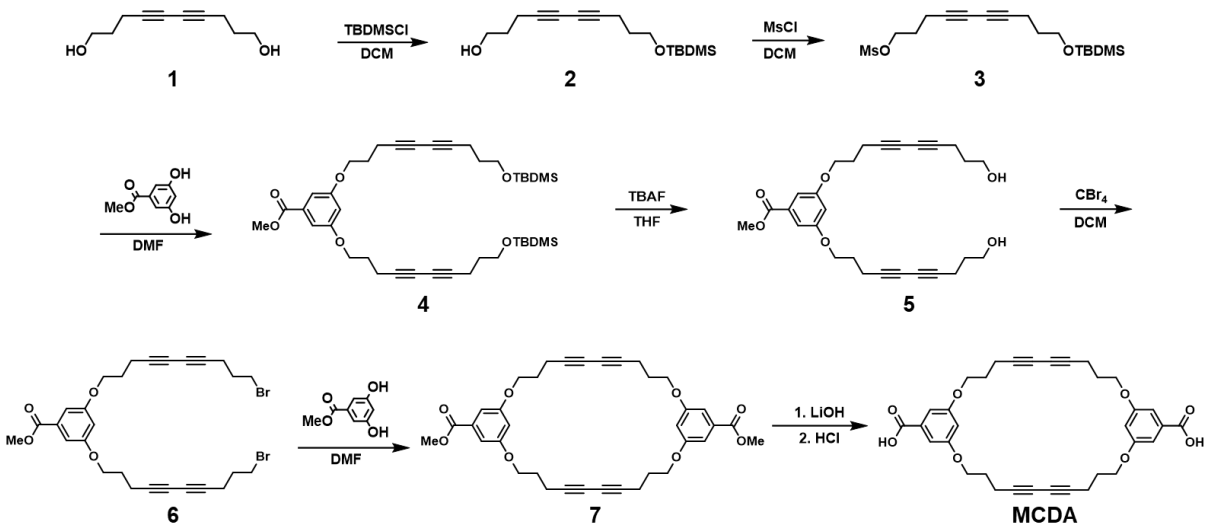

Scheme S1. Synthetic route for macrocyclic diacetylene MCDA.

Intercalation of organic guests in host MCDA. Aqueous dispersion liquid containing 5 mg MCDA (8.8×10^{-3} mmol) was prepared with 0.5 cm^3 purified water in a sonic bath for 30 min. After 0.5 cm^3 purified water was added, the following organic amines (8.8×10^{-3} mmol) was added to the dispersion liquid containing MCDA (Fig. S1): benzylamine (BA, TCI, 99.0 %), 4-methylbenzylamine (Me-BA, TCI, 98.0 %), 4-fluorobenzylamine (F-BA, TCI, 98.0 %), 2-methoxybenzylamine (2-OMe-BA, TCI, 99.0 %), 3-methoxybenzylamine (3-OMe-BA, TCI, 97.0 %), 4-methoxybenzylamine (4-OMe-BA, TCI, 96.0 %), *m*-xylylenediamine (*m*-Xy, TCI, 99.0 %), *p*-xylylenediamine (*p*-Xy, TCI, 99.0 %), 3-thiophenemethylamine (Tp-CH_2NH_2, TCI, 97.0 %), 1-aminododecane (C_{12}-NH_2, TCI, 97 %), 2-(2-aminoethyl)thiophene (Tp-$(CH_2)_2$-NH_2, TCI, 98.0 %), 4-(aminomethyl)benzoic acid (COOH-BA, TCI, 97.0 %), naphthymethylamine (Np-CH_2NH_2, TCI, 98.0 %), 2-phenylethylamine (Ph-$(CH_2)_2$-NH_2, TCI, 98.0 %), 4-aminobenzylamine (NH_2-BA, TCI, 98.0 %), 4-(aminomethyl)phenol (OH-BA, TCI, 98.0 %), (*R*)-(-)-2-phenylglycinol (D-Plgl, TCI, 98.0 %), 4-aminoazobenzen (NH_2-AB, TCI, 98.0 %), 1-(4-cyanophenyl)guanidine (CyPh, TCI, 99.0 %), DL-1-(1-naphthyl)ethylamine (Np-$C(CH_2)NH_2$, TCI, 98.0 %), benzhydrylamine (Ph_2-CH-NH_2, TCI, 97.0 %), aniline (TCI, 99.0 %). The dispersion liquid containing the host and guest was maintained in a sonic bath for 1 h. The molar ratio of these amines to the carboxy group of MCDA was adjusted to 1.0. When the turbid was observed, the precipitates were collected with filtration. Otherwise, the

precipitate was obtained by evaporation of the solvents at room temperature. The resultant MCDA-guests were polymerized with irradiation of UV-LED at 265 nm for 60 s on the temperature-controlled stage at 20 °C to avoid the heating of the sample. As the reference, 30 mg 10,12-pentacosadiynoic acid (PCDA, TCI, 97.0 %), a liner diacetylene monomer, was dissolved in 3 cm^3 chloroform. The molar ratio to the guest amines was adjusted to 1.0. The precipitates were obtained after evaporation of the solvent.

Structural characterization. The intercalation of the guests was studied by Fourier-transform infrared (FT-IR, Jasco FT-IR 4200) spectroscopy and X-ray diffraction (XRD, Bruker D8 Advance) with Cu-Kα radiation. The powdered sample was mixed with KBr for FT-IR analysis. The polymerization behavior was analyzed by Raman spectroscopy (Renishaw, InVia Raman Microscope) with excitation wavelength 785 nm. The morphologies were observed by scanning electron microscopy (SEM, JEOL JSM-7600F) and transmission electron microscopy (TEM, FEI Tecnai G2).

Thermoresponsive color-change properties. The powdered sample between the two glass slides was set on temperature-controlled stages to observe the color-change properties (Linkam, LNP94/2, 10002 with liquid nitrogen in the range of −190 to 300 °C and As-One cool plate in the range of 0 to 100 °C). The samples were heated and cooled at certain temperature. After 30 s, the photographs of the samples were taken for the image analysis using Image-J software. The *R*, *G*, and *B* values were estimated and then converted to *x*, *y*, and *z* values using (eq. S1) an international standard ITU-R BT. 709, (eq. S1).[62] Then, the relationship between *T* and Δ*x* (and Δ*y*) was summarized.

$$\begin{bmatrix} x \\ y \\ z \end{bmatrix} = \begin{bmatrix} 0.4124 & 0.3576 & 0.1805 \\ 0.2126 & 0.7152 & 0.0722 \\ 0.0193 & 0.1192 & 0.9505 \end{bmatrix} \begin{bmatrix} R \\ G \\ B \end{bmatrix} \quad \ldots \text{(eq. S1)}$$

Temperature-dependent UV-Vis spectroscopy was carried out using the powdered sample mixed with KBr for the dilution. The spectra were obtained by a spectrophotometer (Hamamatsu photonics, PMA-12) combined with temperature-controlled stage (Linkam, LNP94/2, 10002 with liquid nitrogen).

Mechanoresponsive color-change properties. The paper-based device of MCDA-(2-OMe-BA) was prepared by filtration of the precursor aqueous dispersion liquid before evaporation of the solvent. MCDA-(2-OMe-BA) homogenously dispersed and fixed on a filter paper was polymerized with irradiation of UV light for 30 s. The PLDA-(2-OMe-BA)-coated paper was prepared by dip-coating of the precursor solution and subsequent topochemical

polymerization, according to the method in our previous work.[58] The cage with weight, total 3109 g, was set on the paper-based devices of PMCDA-(2-OMe-BA) and PLDA-(2-OMe-BA). The temperature was kept at 20 °C to remove the influence of friction heat. The friction force was applied by the tip under the cage. The friction force 7.07 N was applied to four different samples to ensure the reproducibility. The Δx values of the trace area were measured by the image analysis.

Temperature imaging for simulated cryotherapy. The paper-based device of PMCDA-(2-OMe-BA) was used for temperature imaging of the simulated cryotherapy. The paper-based device was set on a temperature-controlled stage at 36 °C. A cotton bud was immersed in liquid nitrogen for 10 s. Then, the cooled cotton bud was immediately attached on the paper-based device for t_{N2} = 1, 2, and 5 s. The processes were recorded by video camera. Then, the time-dependent color-changing behavior was analyzed using the frames. The detailed procedure was described in Fig. S11.

References

(S1) J. M. Heo, Y. Kim, S. Han, J. F. Joung, S. H. Lee, S. Han, J. Noh, J. Kim, S. Park, H. Lee, Y. M. Choi, Y. S. Jung and J. M. Kim, *Macromolecules*, 2017, **50**, 900.

(S2) J. M. Heo, Y. Son, S. Han, H. J. Ro, S. Jun, U. Kundapur, J. Noh and J. M. Kim, *Macromolecules*, 2019, **52**, 4405.

^{1}H and ^{13}C NMR spectra for MCDA

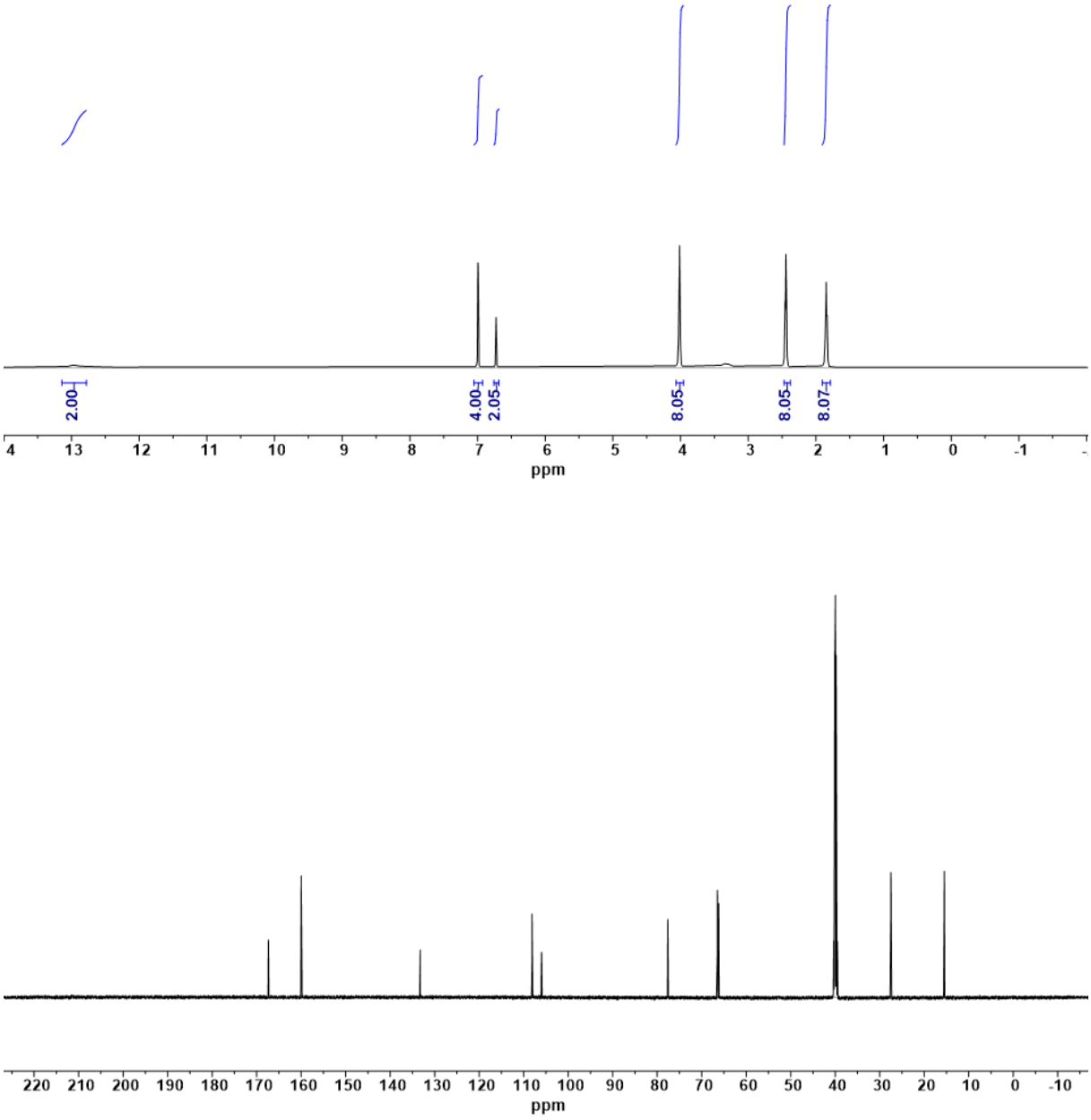

Fig. S1. 1H (top, 600 MHz) and 13C (bottom, 125 MHz) NMR spectra of MCDA in DMSO-d_6.

Guest amines for the intercalation

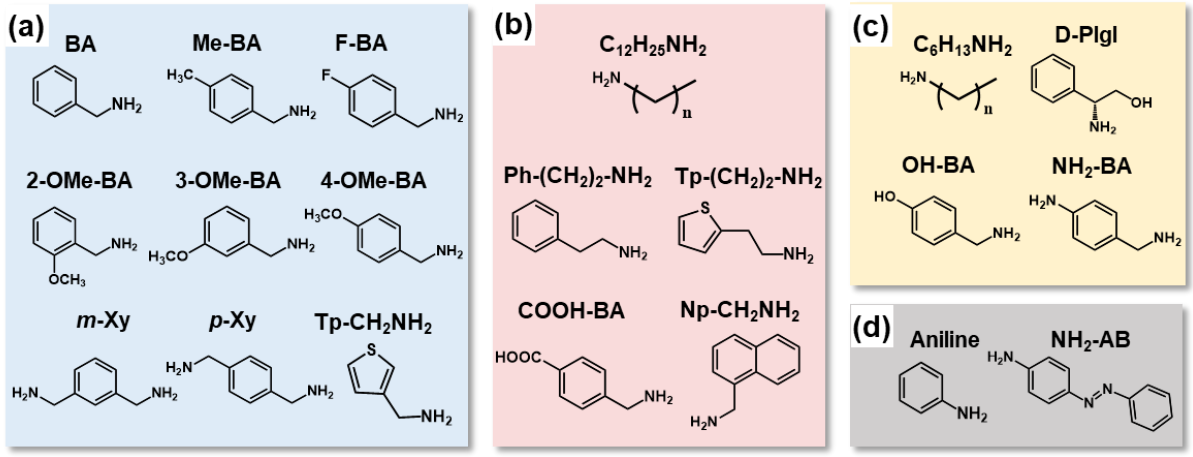

Fig. S2. Molecular structures of the guest organic amines. (a,b) Amines providing the guest-intercalated PMCDAs with blue (a) and red (b) colors. (c) Amines providing the guest-intercalated MCDAs but not polymerized with irradiation of UV light. (d) Aniline derivatives not intercalated.

Benzylamines and their related compound listed in Fig. S2a accommodated in the interlayer space of MCDA and provided the PDA with blue color through the topochemical polymerization (Fig. S3). Whereas the other benzylamines and alkyl amine listed in Fig. S2b were introduced in the interlayer space, the polymerized structure showed the red color. The small molecules can be organized by the stacking with each other in the layered structures. Therefore, the appropriate crystallinity of the layered structures provides the blue PDA with longer effective conjugation length through topochemical polymerization (Fig. S2a). On the other hand, the lower crystalline layered structures are formed by the bulky guest because of the weaker stacking. The red-color PDA with the shorter effective conjugation length was obtained by the amines as shown in Fig. S2b. The coloration of the sample with the polymerization was not observed by the amines in Fig. S2c even with irradiation of UV light. Aniline derivatives were not introduced in the interlayer space because of the weak basicity (Fig. S2d).

Intercalation and polymerization behavior of MCDA

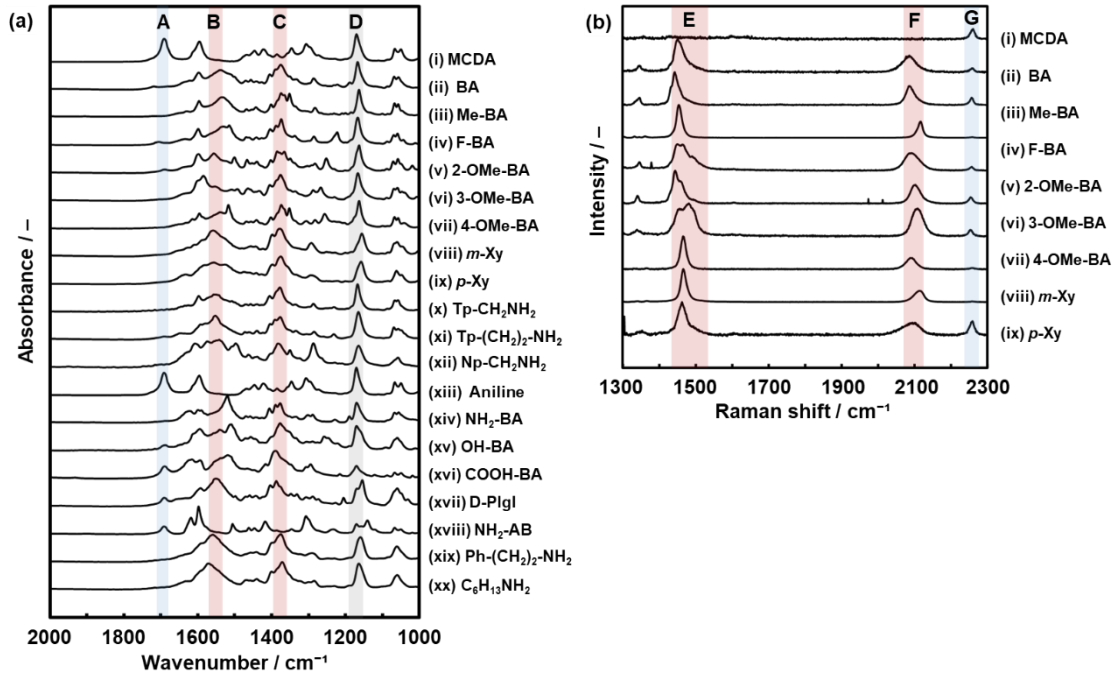

Fig. S3. FT-IR spectra (a) of MCDA with intercalation of the guests and Raman spectra (b) after the UV irradiation.

When the guest molecules were introduced in the interlayer space, the absorption peak corresponding to C=O stretching vibration of the intermolecular dimerized carboxy groups around 1700 cm^{-1} was weakened (band A in Fig. S3a). The peaks corresponding to C=O stretching vibration of monomeric carboxylate group appeared around 1550 cm^{-1} and 1400 cm^{-1} (bands B and C in Fig. S3a). Based on these facts, aniline and NH_2-AB were not intercalated in the interlayer space (the spectra (xiii) and (xviii) in Fig. S3a). The other amines were intercalated in the interlayer space, even though the occupancy was not 100 % for some guests.

Raman spectra were measured only for the PMCDA series exhibiting the blue color (Fig. S1a). The appearance of the bands E and F and weakening of the band G correspond to formation of the ene-yne structure and decrease of the C≡C group, respectively (Fig. S3b). In addition to the coloration, these FT-IR and Raman analyses indicate that the eight guest molecules formed the layered PMCDA.

FT-IR spectra for the detailed characterization

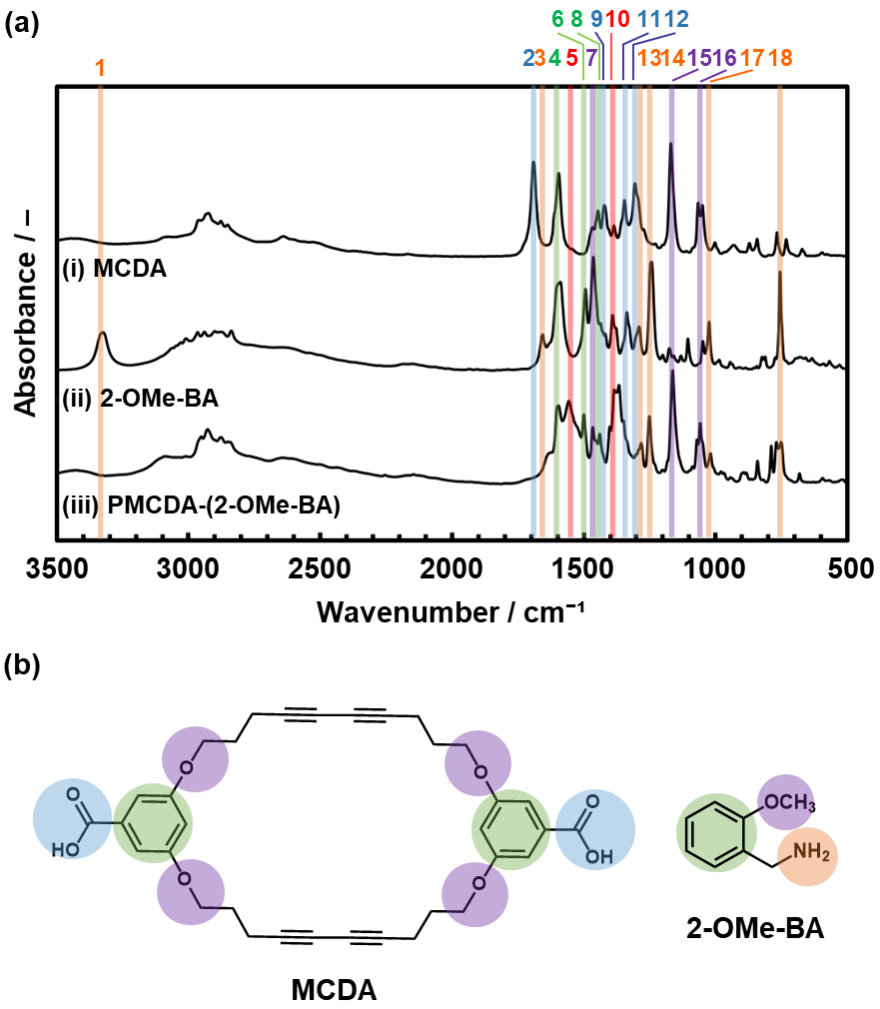

Fig. S4. FT-IR spectra (a) of MCDA (i), 2-OMe-BA (ii), and MCDA-(2-OMe-BA) (iii) and molecular structures for the peak assignments (b).

The colors of the bar and number in the spectra in Fig. S4a correspond to those of the functional groups in the molecular structures in Fig. S4b. All the peaks were assigned to MCDA and 2-OMe-BA as follows: (1) Stretching vibration of N–H in primary amine (3320 cm^{-1}). (2) Stretching vibration of C=O in dimerized carboxy groups (1700 cm^{-1}). (3) Bending vibration of N–H in the primary amine (1650 cm^{-1}). (4) Stretching vibration of C=C in aromatic ring (1600 cm^{-1}). (5) Stretching vibration of C=O in carboxylate anion (1550 cm^{-1}). (6) Stretching vibration of C=C in aromatic ring (1500 cm^{-1}). (7) Bending vibration of C–H in OCH_3 and OCH_2- groups (1480 cm^{-1}). (8) Stretching vibration of C=C in aromatic ring (1450 cm^{-1}). (9) Stretching vibration of C=O in dimerized carboxy groups (1420 cm^{-1}). (10) Stretching vibration of C=O in carboxylate anion (1400 cm^{-1}). (11) Bending vibration of O–H in carboxy group

(1350 cm^{-1}). (12) Stretching vibration of C–O in carboxy group (1300 cm^{-1}). (13) Stretching vibration of C–N in primary amine (1290, 1250 cm^{-1}). (14) Stretching vibration of C–O–C in ethel (1170 cm^{-1}). (15) Stretching vibration of C–O–C in methoxy group (1080 cm^{-1}). (16) Stretching vibration of C–O–C in ethel (1030 cm^{-1}). (17) Stretching vibration of C–N in primary amine (1020 cm^{-1}). (18) Bending vibration of N–H in primary amine (750 cm^{-1}).

XRD patterns of MCDA with the intercalation of the guest

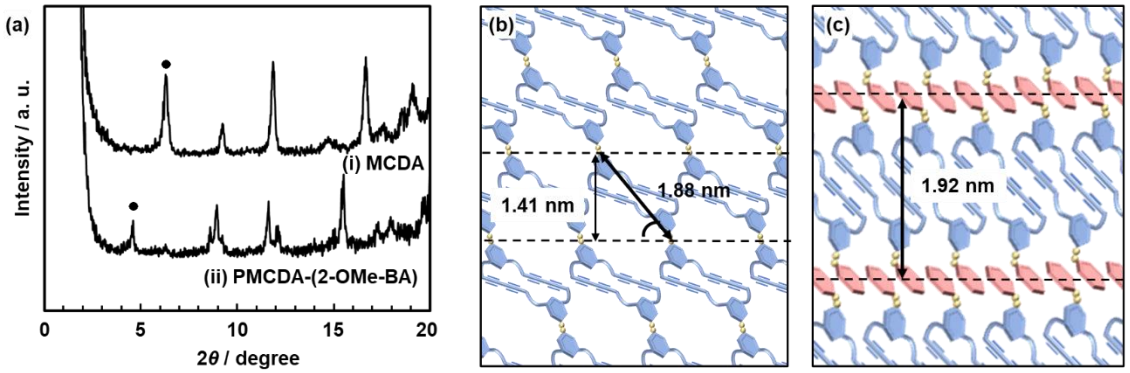

Fig. S5. XRD patterns (a) and schematic illustrations (b,c) of MCDA before (b) and after (c) the intercalation of 2-OMe-BA.

The peaks denoted as by the filled circles correspond to the interlayer distance (Fig. S5a). The peak at 2θ = 6.3 ° was shifted to 4.6 ° after the intercalation of 2-OMe-BA. According to the length of MCDA and 2-OMe-BA,[52] the interlayer distance was estimated to be 1.41 nm for the original MCDA and 1.92 nm for MCDA-(2-OMe-BA) (Fig. S5b,c). After the intercalation of 2-OMe-BA, the conformational change enables the topochemical polymerization of the DA moieties.

Time-dependent intercalation behavior of MCDA

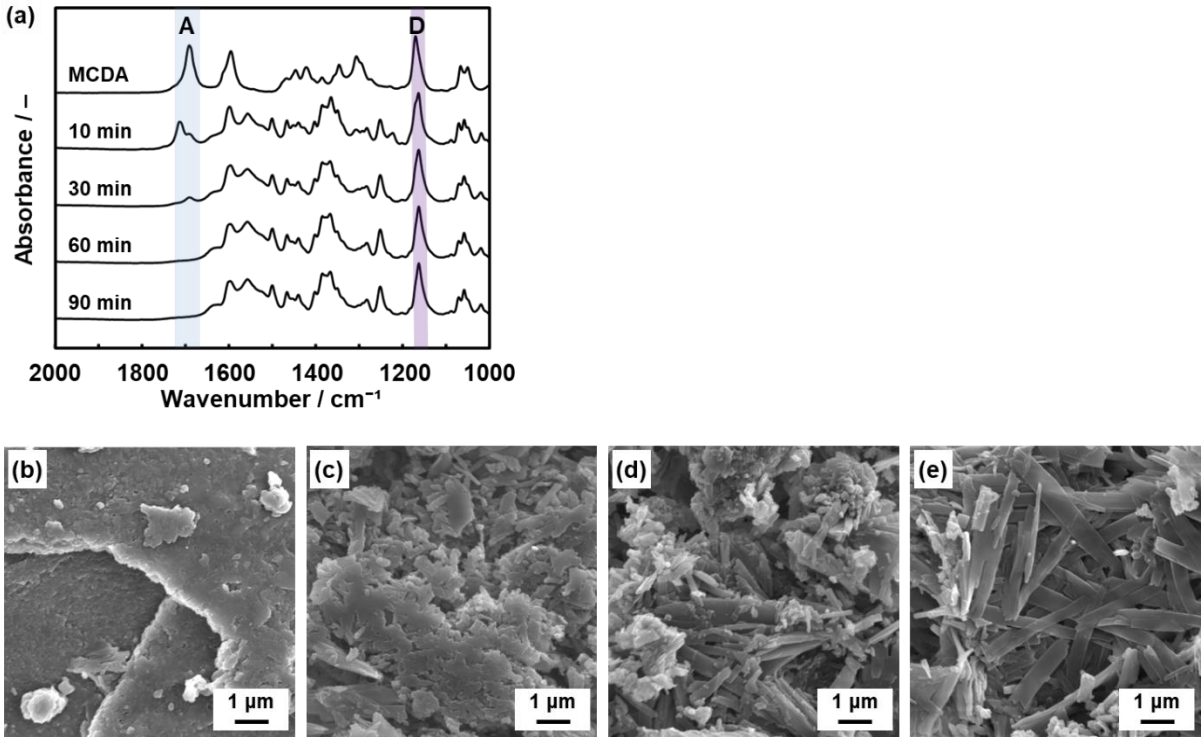

Fig. S6. Time-dependent changes of FT-IR spectra (a) and SEM images (b–e) of MCDA with intercalation of 2-OMe-BA. (a) FT-IR spectra. (b) Original MCDA, (c–e) MCDA with intercalation of 2-OMe-BA for 10 (c), 30 (d), and 60 min (e).

The peaks A and D were assigned to absorption of the stretching vibrations of C=O bond in the dimerized carboxy group and C–O–C bond in the MCDA ring (Figs. 2a and S6a). The absorbance ratio ($R_A = A_{(COOH)2} / A_{C–O–C}$) of the peaks A ($A_{(COOH)2}$) and D ($A_{C–O–C}$) was changed with the time for intercalation. R_A was summarized in Fig. 2d. In addition, the ratio of the nanobelts was increased with an increase in the time for the intercalation (Fig. S6b–e).

Morphologies before the polymerization and after the heating

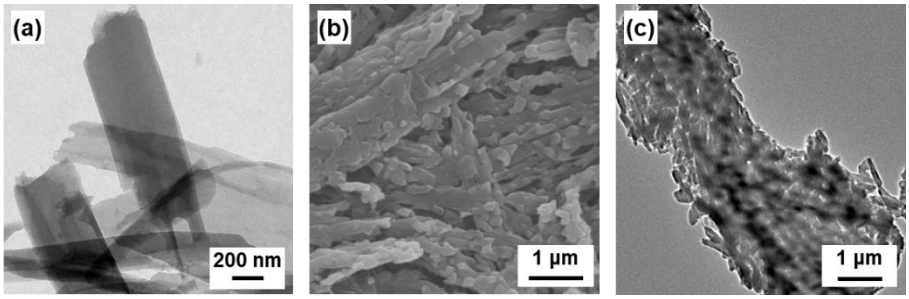

Fig. S7. TEM (a,c) and SEM (b) images of MCDA-(2-OMe-BA) before the polymerization (a) and PMCDA-(2-OMe-BA) after heating at 200 °C.

The morphologies of MCDA-(2-OMe-BA) before the polymerization were not observed because of the polymerization with the sample treatment for the SEM observation. However, the TEM image showed the nanoribbons similar to PMCDA-(2-OMe-BA) (Fig. S7a).

SEM and TEM images of the PMCDA-(2-OMe-BA) sample after the color change to red with heating showed formation of the nanograins in the ribbons (Fig. S7b,c).

Reversibility of the color changes

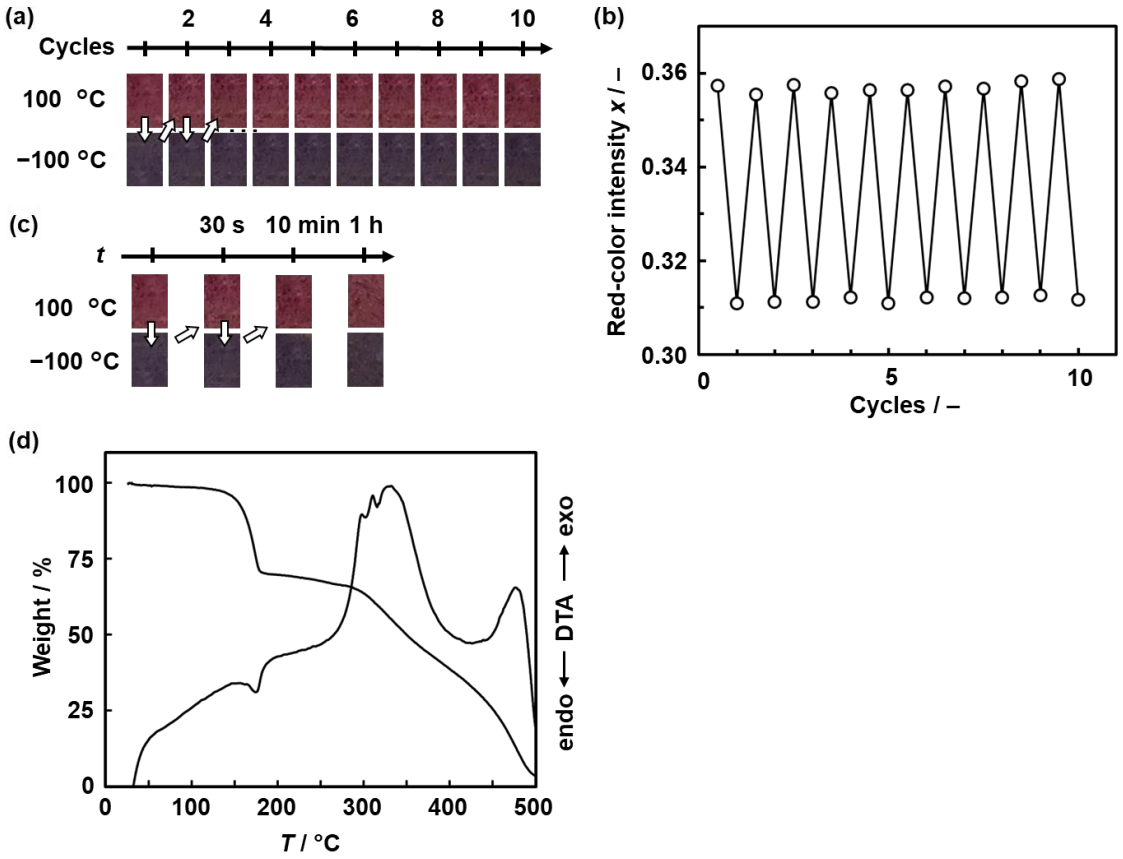

Fig. S8. Reversible color-change properties of PMCDA-(2-OMe-BA). (a) Photographs of the reversible color changes with repetitive heating at 100 °C and cooling at −100 °C for ten cycles. (b) Relationship between the heating-cooling cycles and *x* values. (c) Photographs of the reversible color changes with heating at 100 °C for 30 s, 10 min, and 1 h and subsequent cooling at −100 °C. (d) TG-DTA curves in air atmosphere.

The stable reversible color changes were observed with repetitive heating and cooling (Fig. S8a,b). When the heating time for heating was increased, the reversibility was preserved (Fig. S8c). TG-DTA curves suggest that the guest 2-OMe-BA volatilized with deintercalation around 130 °C (Fig. S8d). The host MCDA layer shows combustion around 290 °C (Fig. S8d). The disappearance of thermoresposivity and reversibility is ascribed to these structural changes of PMCDA-(2-OMe-BA).

Time-course observation of the color changes

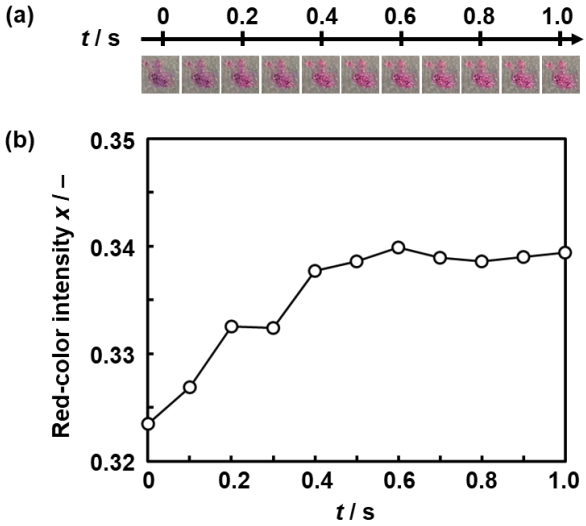

Fig. S9. Time-course color changes of the PMCDA-(2-OMe-BA) powder with heating at 100 °C. (a) Photographs. (b) Relationship between time (*t*) and *x*.

The time-course color changes were observed by dispersion of the sample powder on the temperature-controlled stage at 100 °C (Fig. S9a). The color-changing behavior was recorded as a movie file. The relationship between *t* and *x* indicates that temperature variation was monitored by PMCDA-(2-OMe-BA) in a real time (Fig. S9b). The color change was completed with in 0.5 s upon heating.

Color-change properties of PLDA with intercalation of the guests

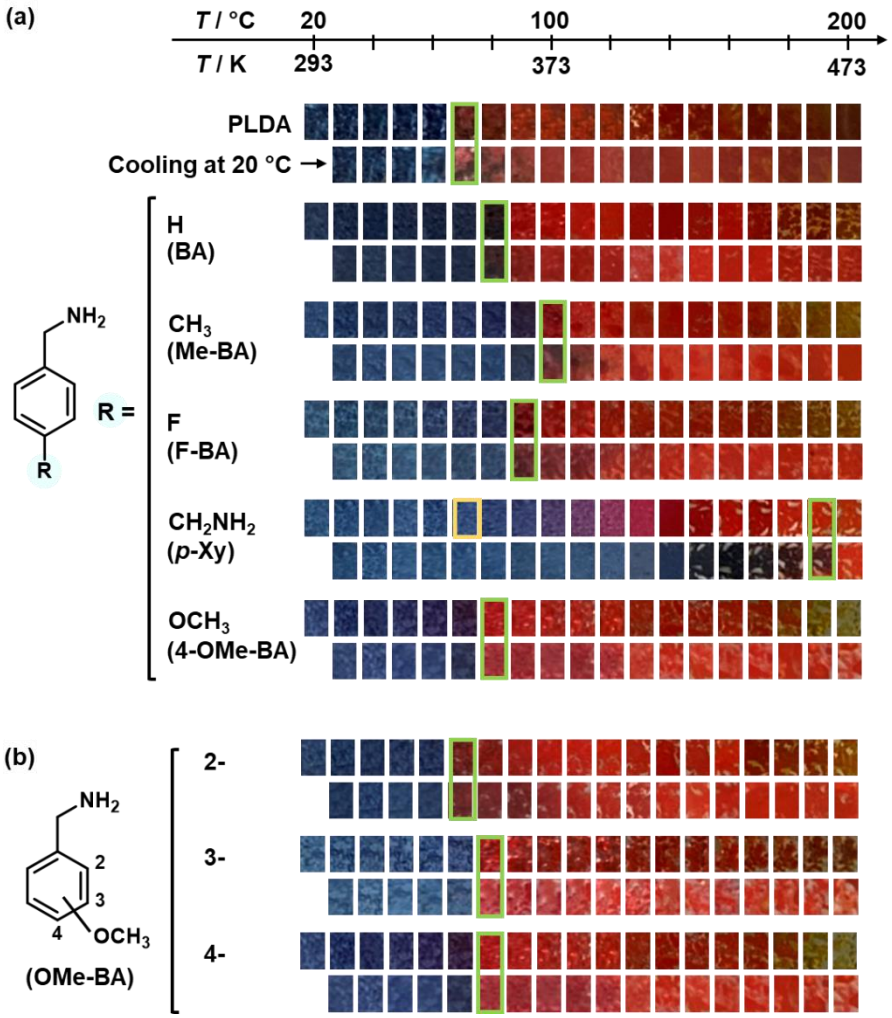

Fig. S10. Photographs of the reference PLDA series with intercalation of the same guests as studied for PMCDA series. (a) Thermoresponsive-color change properties of PLDA-BA, PLDA-(Me-BA), PLDA-(F-BA), PLDA-(*p*-Xy), and PLDA-(4-OMe-BA). (b) Thermoresponsive-color change properties of PLDA-(2-OMe-BA), PLDA-(3-OMe-BA), and PLDA-(4-OMe-BA).

The gradual thermoresponsive color-changing properties with reversibility were not observed for the PLDA series. Although the thermoresponsiveness and reversibility were partially observed for PLDA-(*p*-Xy), the range was narrow compared with those of PMCDA-(2-OMe-BA).

Relationship between *T* and Δ*x* of PMCDA and PLDA with intercalation of guests

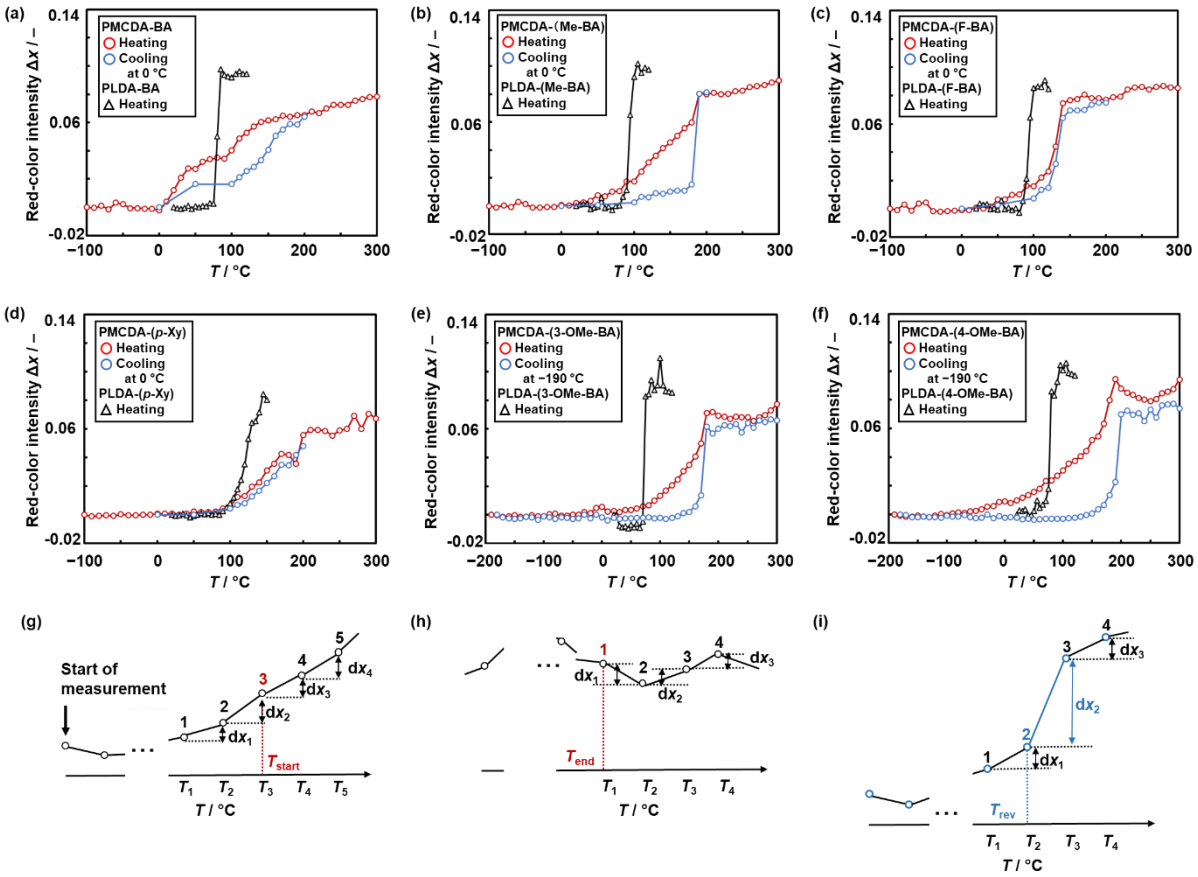

Fig. S11. Relationship between *T* and Δ*x* of PMCDA (red and blue circles) and PLDA (black triangle) with intercalation of the guests (a–f) and definition of T_{start}, T_{end}, T_{rev}, and ΔT_{rev} using the relationship between *T* and Δ*x* (g–i). (a) PMCDA-BA. (b) PMCDA-(Me-BA). (c) PMCDA-(F-BA). (d) PMCDA-(*p*-Xy). (e) PMCDA-(3-OMe-BA). (f) PMCDA-(4-OMe-BA). (g–i) Definitions of T_{start} (g), T_{end} (h), and T_{rev} and ΔT_{rev} (i).

The relationship between *T* and Δ*x* of PMCDA and PLDA series was estimated from the photographs in Fig. 3a,b and Fig. S10 (Fig. S11a–f). The starting temperature of the color change (T_{start}) is defined as follows: When the average value of dx_1, dx_2 and dx_3 and the average value of dx_2, dx_3 and dx_4 are above 0.0005 and 0.001, respectively, T_3 is defined as T_{start} (Fig. S11g). The ending temperature of the color change (T_{end}) is defined as follows: When the differences in the average value of dx_1 and dx_2 and the average value of dx_2 and dx_3 are below 0.001, T_1 is defined as T_{end} (Fig. S11h). The upper limit of the reversible color change (T_{rev}) was defined as follows: When the maximum of dx_n, such as dx_2 in Fig. S11i, is observed, T_2 is defined as T_{rev} (Fig. S11i) and ΔT_{rev} is difference in T_{start} and T_{rev}. According to these definitions, T_{start}, T_{end}, T_{rev}, and ΔT_{rev} were calculated and summarized in Fig. 3a,c, Fig. S10, and Table 1.

Previous studies about thermoresponsive color changes

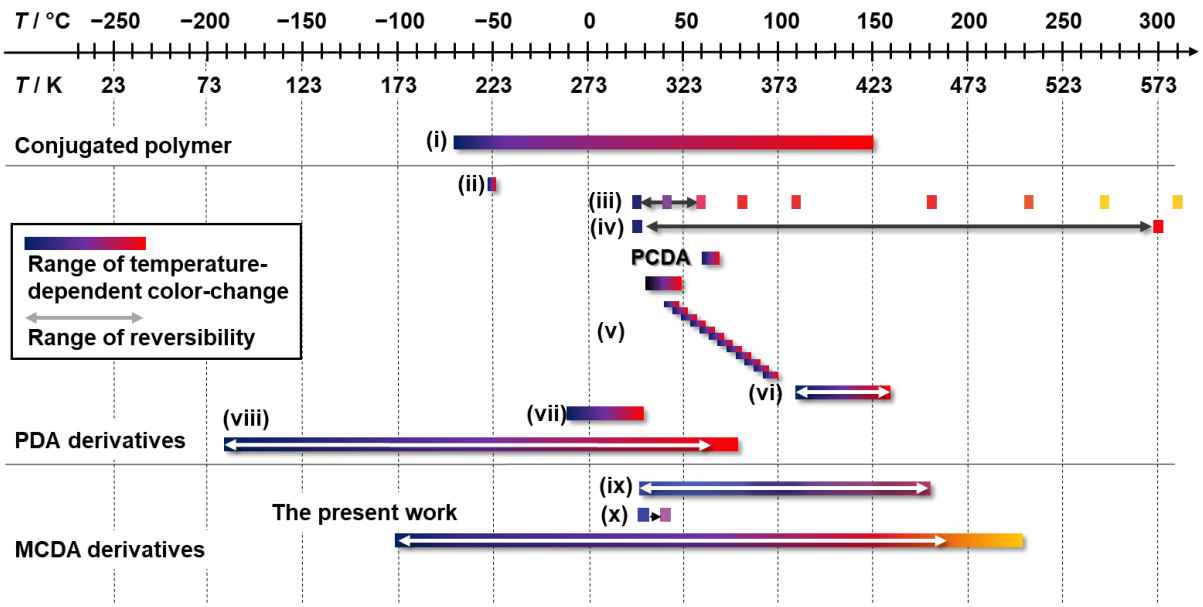

Fig. S12. Temperature range of thermoresponsive color-changing π-conjugated macromolecules, such as polythiophene derivatives (i), PDAs based on designed DA monomers (ii–viii), and PDAs based on macrocyclic DA derivatives series (ix–x), in previous works. The previous works (i–x) correspond to the following references: (i) 63, (ii) 64, (iii) 65, (iv) 66 (v) 58, (vi) 56, (vii) 67, (viii) 59 (ix) 55, and (x) 61.

PMCDA-(2-OMe-BA) shows the widest range of the thermoresponsive and reversible color changes compared with the previous works.

UV-Vis spectra of PMCDA after cooling

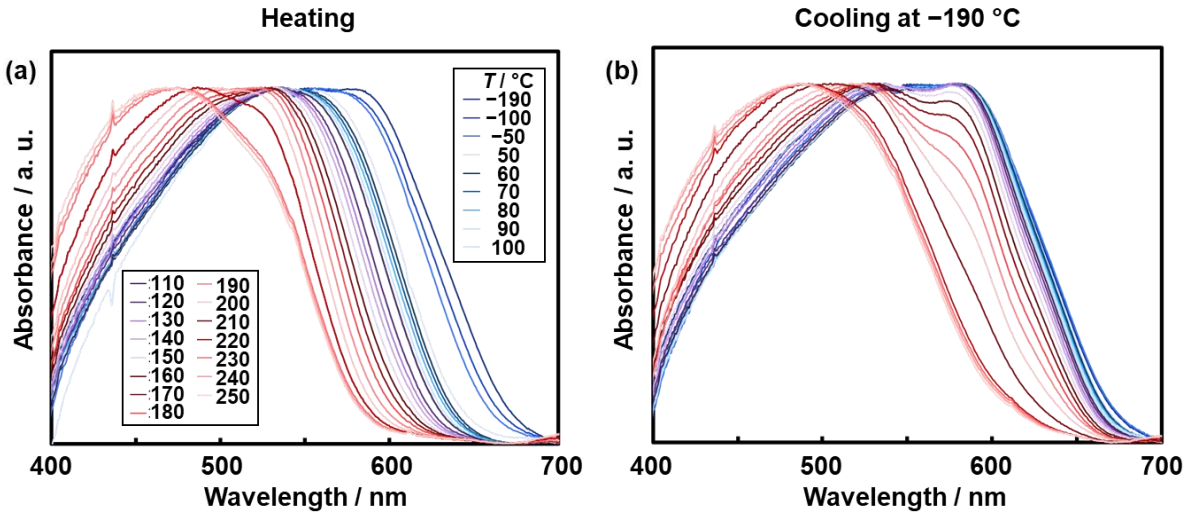

Fig. S13. UV-Vis spectra of PMCDA-(2-OMe-BA) with heating at certain temperature (a) and subsequent cooling at −190 °C (b).

UV-Vis spectra after the heating in the range −180–100 °C recovered to the original positions with cooling at −190 °C. However, the reversibility was weakened after heating in the range 100–190 °C. The spectra were irreversible after heating over 190 °C. The similar reversibility changes were observed on the relationship between T and Δx (Fig. 3d).

Mechanoresponsivity of PMCDA-(2-OMe-BA)

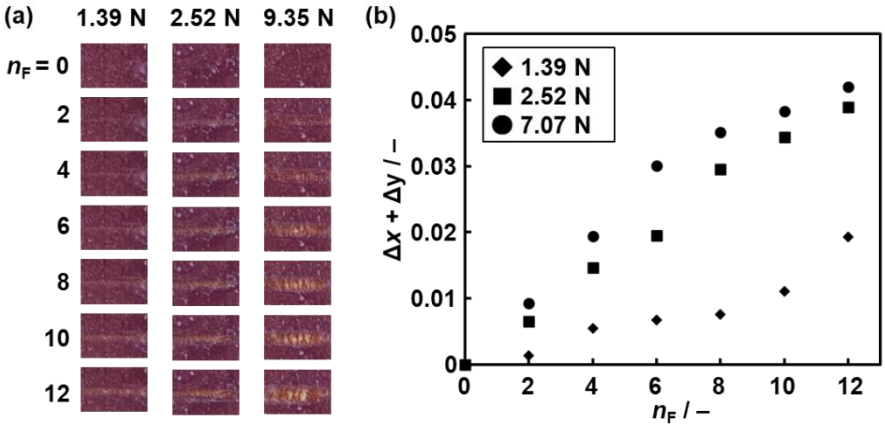

Fig. S14. Mechanoresponsive color-change properties of PMCDA-(2-OMe-BA) with the application of the different friction force (1.39, 2.52, and 9.35 N). (a) Photographs of the color changes at each n_F. (b) Relationship between n_F and $\Delta x + \Delta y$.

The relationship between n_F and $\Delta x + \Delta y$ was obtained when the friction forces 1.39 and 2.52 N, weaker than 7.07 N in the main text (Fig. 4), were applied (Fig. S14b). When the stronger friction force 9.35 N was applied to PMCDA-(2-OMe-BA), the $\Delta x + \Delta y$ values were not accurately estimated from the photographs because of the removal of the PMCDA-(2-OMe-BA) powder from the paper substrates (Fig. S14 in the ESI). On the other hand, the friction force in this range was measured by the color changes of the layered PLDA in our previous works.[58] As the methods for coating on the paper are different in the current and previous works, the stability is different.

Color-change behavior for demonstration of cryotherapy

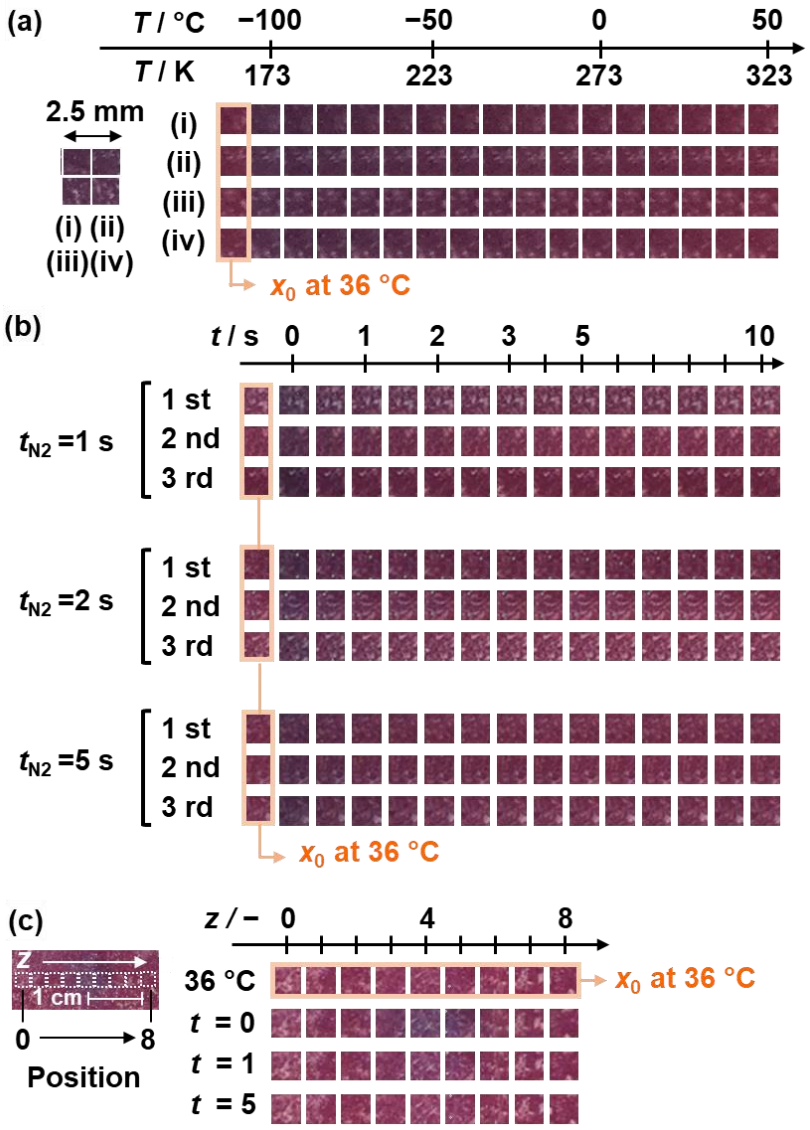

Fig. S15. Original photographs for temperature imaging of the simulated cryotherapy. (a) Photographs of the PMCDA-(2-OMe-BA)-coated paper with changes in temperature for preparation of the calibration curve. (b) Time-dependent color changes of the PMCDA-(2-OMe-BA)-coated paper after stopping the cooling by the cotton buds. The demonstration was carried out three times to ensure the reproducibility. (c) Time-dependent color-changes of the positions 0–8 in the *z* axis.

The *x* values were calculated from these photographs. The x_0 values were defined as the color at 36 °C surrounded by the photographs with the orange frames. The photograph was divided into the frames (i)–(iv) to estimate the average and standard deviation for preparation of the calibration curve, namely relationship between *T* and Δx in Fig. 5b (Fig. S15a). The relationship

between t and average Δx was summarized in Fig. 5d (Fig. S15b). The time-dependent changes in the relationship between the positions 0–8 in the z axis and Δx was summarized in Fig. 5f (Fig. S15c).